Hypodermic-Needle-Like Hollow Polymer Microneedle Array: Fabrication and Characterization

Po-Chun Wang, Seung-Joon Paik, Seong-Hyok Kim, and Mark G. Allen, *Fellow, IEEE*

***Abstract*— A hollow polymer microneedle array with tips and lumens that mimic conventional hypodermic needles, fabricated using UV lithography, and a single-step micromolding technique, is presented for drug delivery into skin. This 6 × 6 needle array consists of 1-mm tall high-aspect ratio hollow microneedles with sharp beveled tips and 150-μm diameter side-opened lumens. A 2-D lithographic mask pattern and the topography of the micromold are utilized simultaneously to define the geometry of the beveled tip and the position of the lumen. Mechanical insertion and fluidic injection characterization of these hypodermic-needle-like (HNL) microneedles (MNs) were performed using excised porcine skin as a substrate. The required insertion force of an HNL MN is 0.275 N, which is comparable with that of a 26-gauge hypodermic needle, 0.284 N. These results are an order of magnitude reduction in insertion force over pyramidal-tip MNs of comparable diameter previously reported by us. This insertion force reduction confirms that the tip geometry is an important factor in utilization of MNs in these applications. No needle fracture was observed under an optical microscope following the pressing of an HNL MN against excised porcine skin with application force of 50 N. Preliminary manual injection of dye through an HNL MN from a syringe into excised porcine skin verified the injection functionality of HNL MNs. [2013-0219]**

***Index Terms*— UV lithography, micromolding technology, SU-8 photoresist, microneedle array, hypodermic needle.**

I. Introduction

HYPODERMIC NEEDLES (HNs) are widely used to deliver a variety of biological molecules into the body through the skin. A sharp beveled tip and a large side opening are key characteristics of HNs, contributing to ease of insertion and efficient, nearly clog-free drug delivery into skin. The sharp tips of HNs are produced by a beveling process, reducing the required penetration force into skin as well as the pain perceived by patients during insertion [1], [2]. The needle lumens, which terminate on the side of the bevel, are expected to be less susceptible to tissue clogging during insertion and form a larger fluid up-take area in the skin [3]–[5].

Manuscript received July 8, 2013; revised October 27, 2013; accepted January 29, 2014. This work was supported by the National Institutes of Health under Grant R01-EB006369 and Grant 1U01AI074579. Subject Editor C. Ahn.

P.-C. Wang and M. G. Allen are with the School of Electrical and Computer Engineering, Georgia Institute of Technology, Atlanta, GA 30332 USA (e-mail: pcwangk@gmail.com; mark.allen@ece.gatech.edu).

S.-J. Paik is with the Institute for Electronics and Nanotechnology, Georgia Institute of Technology, Atlanta, GA 30332 USA (e-mail: spaik8@gatech.edu).

S.-H. Kim was with the School of Electrical and Computer Engineering, Georgia Institute of Technology, Atlanta, GA 30332 USA. He is now with LG Electronics, Seoul 150-721, Korea (e-mail: seonghyok.kim@gmail.com).

Color versions of one or more of the figures in this paper are available online at http://ieeexplore.ieee.org.

Digital Object Identifier 10.1109/JMEMS.2014.2307320

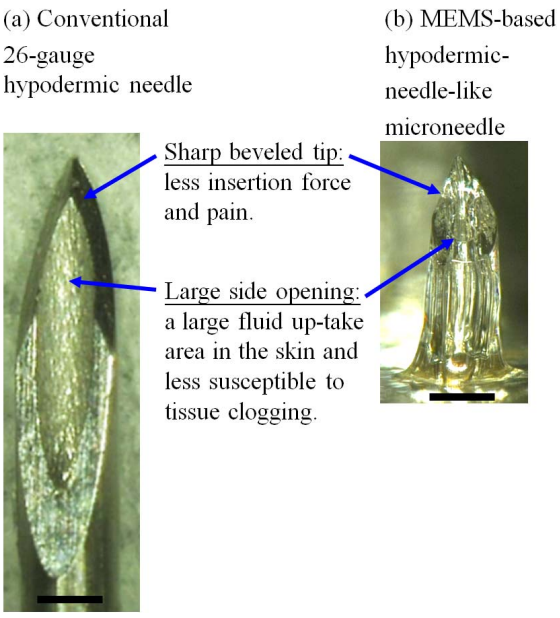

Fig. 1. Optical image of (a) a conventional 26-gauge hypodermic needle and (b) an MEMS-based hypodermic-needle-like microneedle. The major characteristics of a conventional hypodermic needle, a sharp beveled tip and a large side opening, were mimicked in the MEMS-based hypodermic-needle-like microneedle. The scale bar in both (a) and (b) is 300 μm.

Similarly, micromachined needles, or microneedles (MNs), with such side-terminated lumens exhibit superior fluid delivery performance over MNs with a top-terminated lumen [3]. Fig. 1(a) shows an optical micrograph of the needle tip of a conventional 26-gauge (26G) hypodermic needle (HN), showing the sharp beveled tip and large side-terminated lumen opening.

MNs have been reported to successfully transport biological molecules into the body with minimal invasiveness and pain, following the insertion of needles into the skin [6]. Biological molecules delivered through microneedles (MNs) into the skin have been shown to induce immune responses or biological effects that are comparable to those induced by an HN injection in animal and human studies [7]–[11]. Other advantages of MNs are the potential for non-skilled/self-administration, blood-free insertion, minimal skin trauma, ease of disposal, and reduced risk of needle-stick injury [12], [13].

Therefore, integration of the two key characteristics of HNs, namely sharp beveled tip and large side opening, into the design of MNs can potentially lead to enhanced MN performance. An optical micrograph of the fabricated HNL MN, presented in this paper, with a sharp beveled tip and a large side opening is shown in Fig. 1(b).

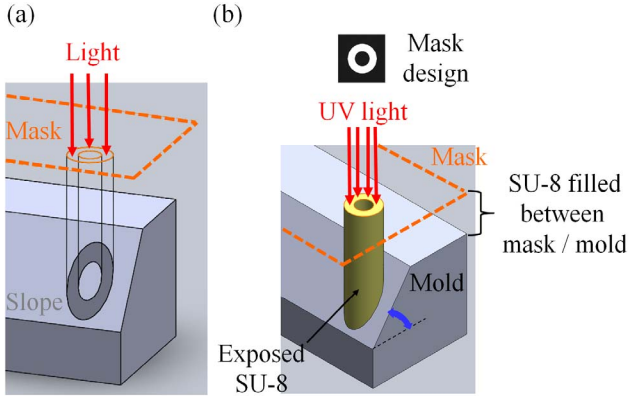

Fig. 2. (a) Projection of a two-dimensional mask pattern onto a three-dimensional surface. (b) Illustration of the construction of a microneedle structure by a combination of UV exposure and the topography of a mold.

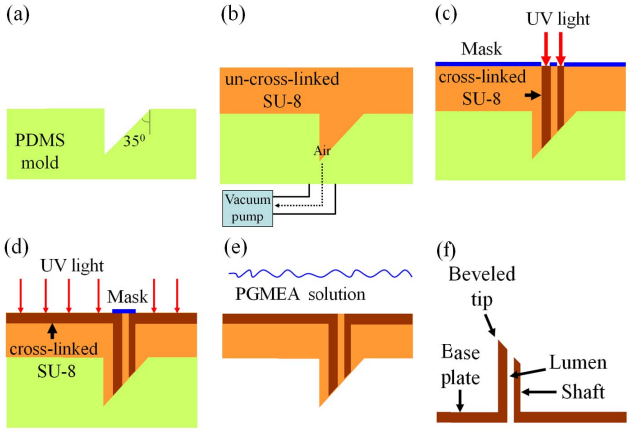

Fig. 3. Fabrication process flow of the hypodermic-needle-like microneedle structures. The UV dosage in step (c) is 1800 mJ/cm^2, and that in step (d) is 350 mJ/cm^2.

To construct the hypodermic-needle-like tip geometry of MNs, several fabrication approaches have been reported. Anisotropic etching of silicon yielded a beveled tip with a fixed bevel angle due to the nature of the crystalline structure in silicon [14]. Beveled tips can also be achieved using serial saw dicing on high-aspect-ratio silicon tubes fabricated with silicon dry etching [15]. Laser micromachining was used to create beveled tips out of tapered nickel tubes fabricated using drawing lithography with SU-8 and electroplating of nickel onto the drawn SU-8 [16]. Deep X-ray lithography with double orthogonal exposure was reported to construct polymer MNs with beveled tips and side openings [17]. In these approaches, multiple complex process steps, serial processes, or facilities with limited availability were involved to achieve sharp beveled tips.

Batch processing capable of creating three-dimensional structures using readily available equipment is desired for the manufacturing of MNs that serve as single-use devices [18]. A combination of conventional UV lithography and a single-step molding technique can achieve the goal of beveled tips and side-terminated lumens. Several attempts to realize these structures using this approach have been made. Beveled-tip SU-8 MNs of 430 μm in height were fabricated using a silicon mold [19]. Between MNs, additional access holes on the back plate were created to assist in the process of development and release. The bevel angle of MN tips was fixed since the silicon mold was constructed using anisotropic etching into silicon. Fabrication of 980 μm tall HNL MNs with a functional baseplate based on UV lithography of SU-8 in elastomeric polymer molds was presented in [20]. The use of elastomeric molds not only allowed for ease of separation of the optically-defined microneedles from the molding substrate, but also allowed the bevel angle of the MN tips to be modified, since the elastomeric mold used was constructed using an inclined UV lithography process with an adjustable incline angle. More recent work using UV lithography of SU-8 in silicon molds has proposed [21] and demonstrated [22] extension of the previous silicon mold work to heights of approximately 1000 μm.

The fabrication concept for the combination of conventional UV lithography and a single-step micromolding technique to construct HNL MNs is shown in Fig. 2. As shown in Fig. 2(a), when light perpendicularly illuminates the photomask, a circular pattern on the mask is projected onto the slope of the mold, creating an elliptical shape on the slope. By changing the pattern on the mask, various projected shapes on the sloped sidewall of the mold can be obtained. With a negative photoresist (e.g., SU-8) filling the region between the mask and the mold, the beveled tip, lumen, and shaft of an HNL MN can be defined simultaneously with a single UV exposure, Fig. 2(b). The angle of the slope of the mold defines the bevel angle of the MN tips and can be altered during the construction of the mold, and the sharpness of the tip can be defined lithographically. This combination of UV lithography and micromolding allows the geometry of the MN tip to be optimized three-dimensionally with two dimensions from the design of the mask pattern and one dimension from the slope angle of the mold.

II. Microneedle Fabrication

The fabrication process of the HNL MN array started with a pre-constructed, reusable polydimethylsiloxane (PDMS) mold. The construction of this PDMS (Sylgard 184, Dow Corning, Midland, MI, USA) mold involved the use of an inclined UV lithography process [23] to create an SU-8 master, followed by a two-step micromolding technique to replicate this SU-8 master in PDMS [18], [24]. The ultimate PDMS mold comprised a 6 $\times$ 6 array of square recesses. Each recess measures approximately 500 $\times$ 500 μm with 900 μm spacing between recesses. The cross-section of each recess is a right-angled triangle, as shown in Fig. 3(a), 715 μm in depth. Following the construction of the PDMS mold, the fabrication process flow of an SU-8 HNL MN on the constructed PDMS mold is shown in Fig. 3. A quantity of SU-8 2025 (MicroChem Corp., Newton, MA, USA) was first preheated at 60 °C for 30 minutes on a hotplate in order to reduce its viscosity for better encapsulation of the micro-trenches in the PDMS mold. The top surface of the PDMS mold was treated using oxygen plasma for 20 minutes to increase its hydrophilicity prior to the SU-8 encapsulation. Following the surface treatment of the PMDS mold, the preheated SU-8 was cast manually by weight

onto the PDMS mold to obtain a thickness of 600–650 μm. To eliminate trapped air bubbles in the PDMS trenches during the casting process, a backside vacuuming (BSV) process was performed for one hour, as shown in Fig. 3(b). In the BSV process, because of the gas permeability of PDMS [25], the air trapped at the bottom of the PDMS trenches was drawn through the PDMS mold and subsequently purged. The SU-8/PDMS sample was then placed on a hotplate at 85 °C for 16 hours to soft bake the SU-8.

To define an HNL MN array with a baseplate, a UV (365 nm, I-line) lithography process, consisting of two exposure steps with separate masks, was used. The beveled tip, lumen, and shaft of an HNL MN were defined simultaneously by the first exposure with a UV dosage of 1800 mJ/cm^2, as shown in Fig. 3(c). A post-exposure-bake (PEB) step was then performed on a hotplate at 85 °C for 30 minutes. Prior to development, the baseplate of the HNL MN array was formed using a second exposure with a reduced UV dosage of 350 mJ/cm^2 and a mask that blocked the needle lumens and shafts from the exposure, as shown in Fig. 3(d). For faster heat transfer to the baseplate located on the top of the SU-8/PDMS sample, the second PEB process was carried out in an oven, instead of a hotplate, at 85 °C for 15 minutes.

The SU-8 structure was then demolded from the PDMS mold and held in a static propylene glycol methyl ether acetate (PGMEA) bath with both openings of the lumen in contact with the PGMEA (Microposit Thinner Type P, Rohm and Haas Electronic Materials, Marlborough, MA, USA) solution for six hours to develop the SU-8, as shown in Fig. 3(e). Following the development, the sample was gently blown dry using a nitrogen gun. The developed HNL MN with a baseplate is shown in Fig. 3(f). To complete the fabrication, both sides of the SU-8 MN array were UV-flood exposed with a UV dosage of 10 J/cm^2, followed by a hard bake of the SU-8 on a hotplate at 135 °C for 30 minutes. Detailed process improvements, including compensation for the thermal expansion of the PDMS mold with photomask design, were discussed in [18].

Three different mask designs, their resultant expected MN shapes as determined from projection CAD, and fabricated MNs, are shown in Fig. 4. The bevel angle of the MN tips is 35° in all three CAD drawings. The fabricated HNL MN shown in Fig. 4(c) is 980 μm tall with a 300 μm wide shaft. The distance between the lumen opening and the baseplate is 590 μm. The diameter of the lumen opening is 150 μm. The mask design in Fig. 4(c) was selected to construct HNL MNs for further characterization discussed in this paper.

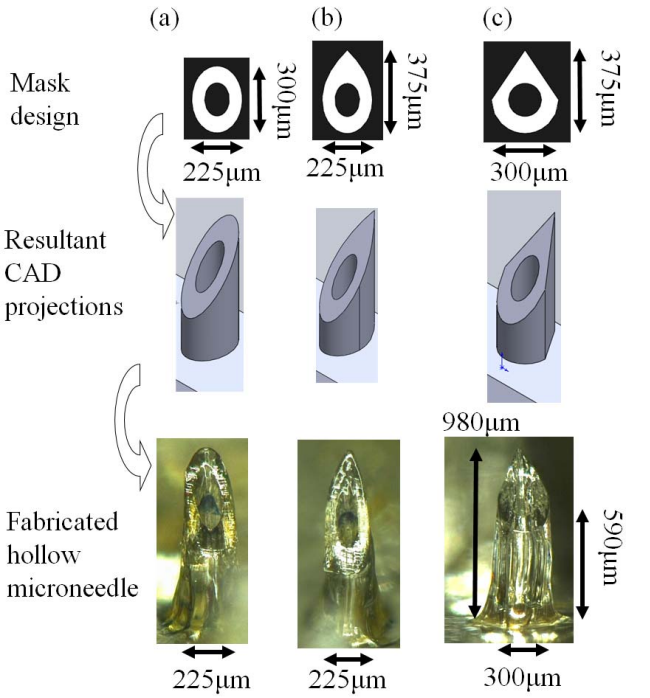

Fig. 4. Three different mask designs, resultant CAD projections of three microneedle tips from each designs, and optical micrographs of corresponding fabricated hollow microneedles.

III. Characterization of Microneedles

A. Preliminary Testing of Microneedle Array

The skin penetrability of the fabricated HNL MNs, as shown in Fig. 4(c), was assessed with excised porcine skin. The excised porcine skin (Pel-Freez, Rogers, AR, USA) was shaved using a razor to trim the hairs on the skin. Subcutaneous fat on the back of the skin was subsequently removed with a scalpel. The resultant porcine skin was 3–4 mm in thickness. The prepared skin was then mounted under mild tension onto a wooden block using screws. The baseplate of a 6 × 6 MN array was affixed to the center of the plate of a scanning electron microscope (SEM) specimen mount using double-sided tape. To insert MNs into the porcine skin, the MN array was then pressed perpendicularly against the skin by manually pushing the SEM mount toward the skin, followed by separation of the array from the skin. Successful insertion of needles into skin was defined as creation of an opening through the stratum corneum (SC) layer, the outmost layer of skin and a substantial barrier to essentially all high-molecular-weight drugs [12], [26]. To confirm the openings in the SC, one drop of blue dye was dispensed onto the skin surface. The dye flowed through the MN-defined pathways, if created as a result of successful insertion, in the SC and stained the viable epidermis (VE) underneath. Stain in the VE serves as an indication of successful insertion of the MN into the skin. The residual dye on the skin surface was then removed using alcohol swabs. The skin surface was examined under an optical microscope.

Fig. 5(a) shows an optical micrograph of the top view of the insertion area on the porcine skin following the insertion test. In Fig. 5(a), thirty-five stains in the VE can be easily identified, indicating 35 successful insertion loci out of the fabricated 6 × 6 needle array. The failed insertion point on the upper right corner of the array corresponds to a broken tip of the MN observed prior to the insertion test. A close-up view of an insertion site is shown in Fig. 5(b). The red triangle at the center indicates the pathway created by successful insertion of a MN into skin, and the black circle highlights the region where the dye diffused and stained the VE underneath the SC. The side view of the same MN prior to and following insertion

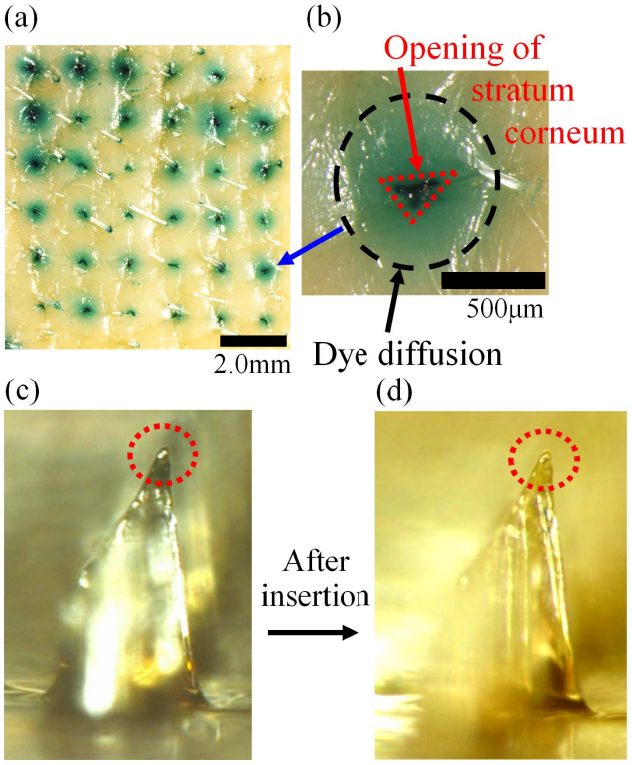

Fig. 5. (a) An optical micrograph of the excised porcine skin following the manual insertion of a 6 × 6 microneedle array. (b) A close-up view of an insertion site, showing the opening in the stratum corneum created by needle insertion and the dye diffusion in the viable epidermis underneath the stratum corneum. (c)(d) Optical micrographs of the side-view of the same microneedle prior to and following manual insertion into skin, respectively. The dashed red circles highlight the needle tip.

are shown in Fig. 5(c) and (d), respectively. No visible damage to the MN or bending of the MN tip was observed under an optical microscope after the insertion.

To verify the lumens are well-defined inside the fabricated MNs and baseplate, a microfluidic channel test of the fabricated HNL MN array was carried out using a custom package and fluid test setup discussed in [27]. In the test, a syringe pump drove the blue dye in a syringe at a flow rate of 2.0 ml/min through the tubing, a PDMS housing, a dye reservoir, and then any well-defined lumens in the MN array, followed by the dye being ejected from the MN array in streams. Fig. 6 shows an optical image of the custom package and dye streams ejected from the MN array. The number of the ejected dye streams corresponds to the number of well-defined lumens. Therefore, the observed dye streams in Fig. 6 indicated at least 85% of the lumens were open.

B. Biological Insertion Characterization of Microneedles

Mechanical interaction characterization of the HNL MNs was performed by driving individual HNL MNs perpendicularly against excised porcine skin. The required driving force for an HNL MN to successfully insert into skin, which is defined as insertion force, was evaluated. The maximum driving force that can be applied to an HNL MN during insertion without needle fracture was estimated.

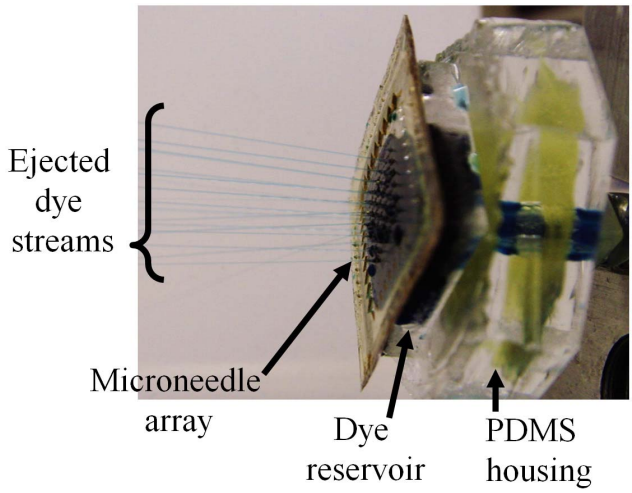

Fig. 6. Optical still image of dye streams ejected from a microneedle array attached to a custom package in a microfluidic channel test. Eighteen visible streams ejected from an array of 21 hollow microneedles, suggesting an open lumen yield of 85%.

To evaluate the insertion force for single HNL MNs, an HNL MN array with a baseplate was coated with 15 nm of chromium and 150 nm of gold using a sputterer for skin resistance measurement [18] with which the insertion force was determined. An individual HNL MN with its surrounding baseplate was cut from the MN array using a razor blade and then mounted onto the bottom surface of a flat-head steel machine screw. The machine screw was affixed to the center of the plate of an aluminum SEM specimen mount for ease of handling. For insertion force measurement of HNs, a 26G HN was directly mounted to an aluminum SEM specimen mount with the needle hub affixed to the center of the plate.

A force-displacement test station (Model 921A, Tricor Systems Inc., Elgin, IL, USA) with a built-in ohmmeter was used to perform the insertion test. An individual needle was driven perpendicularly against excised porcine skin at a rate of 1.0 mm/s by the load cell of the test station. The test station simultaneously recorded the driving force and displacement of the needle as well as the skin resistance between the needle and the electrode gel that was applied to the skin surface 1-2 inches away from the insertion site. An abrupt decrease in the skin resistance indicated the rupture of the highly-resistive SC layer, which defines successful insertion into skin. The driving force corresponding to the abrupt skin resistance decrease is taken as the insertion force of the needle. Detailed descriptions of the preparation of individual needles and excised porcine skin as well as the experimental setup and test methodology were discussed in [18].

Eight individual HNL MNs were tested with each needle inserted into skin one or two times, yielding 14 data points for the insertion force. The mean of these 14 data points is 0.275 N with a standard deviation (SD) of 0.113 N. For the insertion force measurement of HNs, two conventional 26G stainless-steel HNs were used and 28 data points were obtained. The mean of the 28 data points is 0.284 N with a SD of 0.059 N. Fig. 7 shows a chart of the insertion force for 26G HNs and HNL MNs with the mean, SD, maximum and minimum

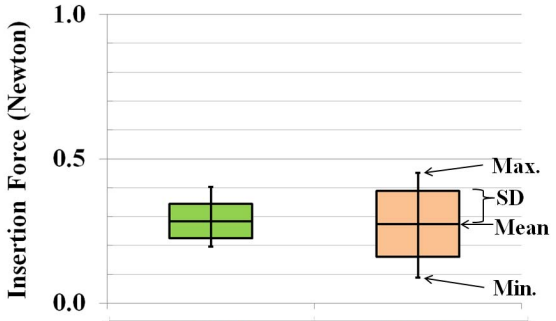

	26G HN (28 data pt. 2 HNs)	HNL MN (14 data pt. 8 MNs)
Mean	**0.284**	**0.275**
Standard Deviation (SD)	**0.059**	**0.113**
Max.	0.402	0.451
Min.	0.196	0.088

Fig. 7. A chart showing the insertion force of 26-gauge hypodermic needles and hypodermic-needle-like microneedles. The mean, standard deviation, maximum, and minimum of all obtained data points are shown for both types of needles. The mean insertion force of hypodermic needles and microneedles is 0.284 N and 0.275 N, respectively, indicating that hypodermic-needle-like microneedles exhibit comparable insertion performance to hypodermic needles.

of obtained data points. The insertion force of HNL MNs is comparable to that of conventional 26G HNs, indicating that HNL MNs exhibit comparable insertion performance to 26G HNs.

The insertion forces measured for HNL MNs are significantly lower than the previously-fabricated pyramidal-tip (PT) MNs, which were constructed using a similar fabrication approach but had a different tip geometry [18]. The insertion force of a PT MN into excised porcine skin was characterized as 2.4 N, which is approximately nine times higher than that of an HNL MN. The tip diameter of a PT MN ranges from 15 μm to 25 μm [27]. Preliminary characterization using a high-magnification (2500X) optical microscope showed that the tip diameter of HNL MNs is $\sim$30μm. The comparison of PT MNs and HNL MNs in the insertion force and tip diameter showed that the change of tip geometry from a pyramidal shape to an HNL one reduced the insertion force by approximately one order of magnitude with comparable tip diameters, indicating that the tip geometry is an important factor in utilization of MNs in the applications of drug delivery into skin.

To estimate the margin of safety, the fracture force of HNL MNs was characterized using excised porcine skin, the same substrate as in the insertion test. Three HNL MNs were tested using another force-displacement test station (ElectroForce 3200 Test Instrument, Bose Co., Eden Prairie, MN, USA) in order to increase the maximum driving force in the test. Similar testing procedures were performed as in the insertion test with an increased maximum driving force of 50 N. Following the test, successful insertion of each needle into skin was confirmed with the examination of the skin staining under an optical microscope. In all three tested HNL MNs, minor bending of the needle tip was observed under an

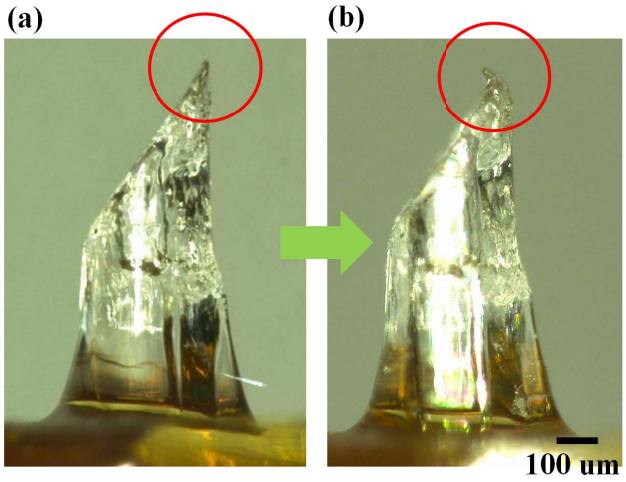

Fig. 8. Optical micrographs of the side view of a hypodermic-needle-like microneedle (a) prior to and (b) following the fracture force test with 50 N force application against excised porcine skin. Minor bending of the needle tip was observed following the test. No fracture of the needle structure was observed. The scale bar in (b) is 100 μm.

optical microscope after the 50 N force application. Optical micrographs of the side view of one tested needle prior to and following the fracture test are shown in Fig. 8(a) and (b), respectively. No fracture of the needle was observed in all three needles, indicating that the fracture force of the needle for insertion into porcine skin is in excess of 50 N. With the fracture force higher than 50 N and the mean insertion force of 0.275 N for HNL MNs, the margin of safety for needle insertion into porcine skin prior to needle fracture is at least 180 [28].

C. Microfluidic Characterization of Microneedles

Fluid resistance is important in estimating the required pressure to drive fluid through a fluid channel at a given flow rate. Both theoretical calculation and empirical characterization of the fluid resistance of a lumen inside an HNL MN and the baseplate were performed.

Theoretical calculation of the fluid resistance of a lumen was carried out using the Poiseuille equation [29],

$$\Delta P = \frac{128 \mu L Q}{\pi d^4} \tag{1}$$

where ΔP is the fluid pressure, Q is the volumetric flow rate, μ is the dynamic viscosity of the fluid, L is the length of fluid channel, and d is the diameter of the fluid channel. With a Q of 1.0 ml/min, μ of 8.9×10^{-4} Pa-sec for water at 25 °C, L of 0.790 mm, and d of 0.150 mm, the fluid pressure was calculated to be 940 Pa, resulting in a theoretical fluid resistance of 940 Pa/(ml/min).

The fluid resistance of a lumen was empirically determined using a custom fluid system. The custom fluid system involved a three-way fluid adapter. One opening of the adapter was connected to a 10 ml syringe through tubing. The syringe was filled with water and driven by a syringe pump at a constant flow rate of 1.0 ml/min. Another opening of the adapter was directly connected to a manometer (DigiMano 220, Netech, Farmingdale, NY, USA), which measured the fluid pressure.

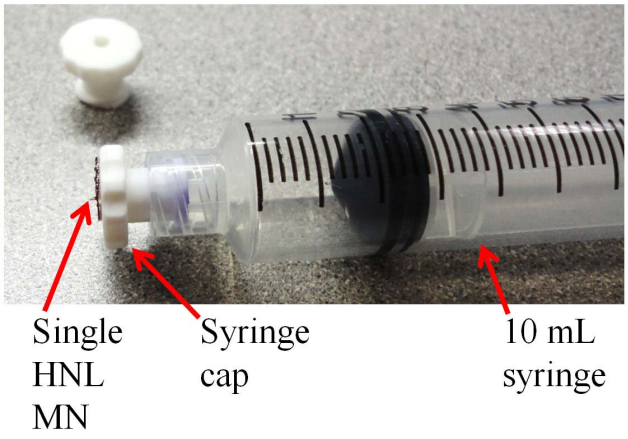

Fig. 9. Optical image of the custom single-HNL-MN injection system. An HNL MN with its surrounding baseplate was attached to a center-drilled syringe cap, which was mounted to a 10 ml syringe. Another center-drilled syringe cap is shown in the upper left corner of this image.

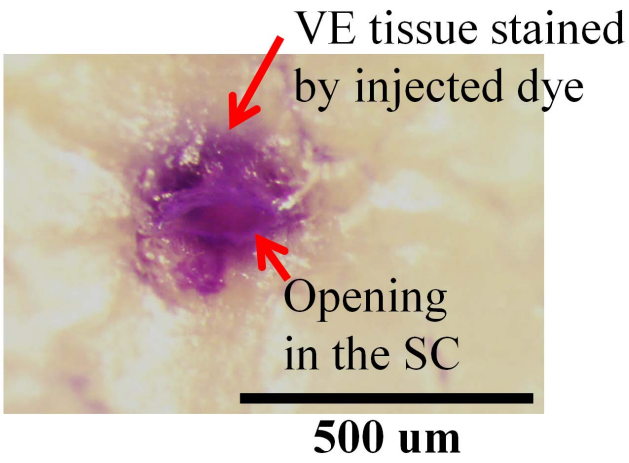

Fig. 10. Optical micrograph of the top view of an insertion/injection site on the excised porcine skin following the insertion of an HNL MN and the injection of dye through the HNL MN. The opening in the stratum corneum (SC) was caused by the successful insertion of the needle, followed immediately by dye injection through the HNL MN. The injected dye stained the viable epidermis (VE) underneath the SC.

The last opening was connected to the back of the baseplate of an HNL MN through tubing. Initially the tested HNL MN was not attached to the tubing. With a constant flow rate of 1.0 ml/min from the syringe pump, the fluid pressure at the adapter was negligible since it was below the accuracy of the manometer. With the HNL MN attached to the tubing, the fluid pressure at the adapter increased to 5600 Pa. Therefore, with a flow rate of 1.0 ml/min, the fluid resistance was 5600 Pa/(ml/min). Although higher than theoretically predicted, it is instructive to compare this result with the pressure required to inject fluid through hollow MNs into skin *in-vivo*. The fluid pressure required for saline injection into live human skin through a glass hollow MN at a flow rate of 1.0 ml/min was empirically characterized to be 10-80 psi (70-550 kPa) [30]. Therefore, the fluid pressure introduced by an HNL MN is negligible in comparison to the required pressure for fluid injection through MNs into live human skin at the flow rate of interest, i.e. 1.0 ml/min.

A preliminary injection test was performed manually using a custom single-HNL-MN injection system, as shown in Fig. 9, with excised porcine skin. To construct the custom injection system, an HNL MN with its surrounding baseplate was cut from an HNL MN array using a razor blade. A syringe cap was drilled at its center to open a fluid channel through the cap. The MN sample was affixed to the syringe cap with the opening of the MN lumen aligned within the center opening of the syringe cap. The syringe cap was then directly connected to a 10 ml syringe filled with dye.

To inject the dye into skin, the syringe was held perpendicularly to the skin surface by hand and then moved toward the skin to insert the HNL MN into skin. Following the insertion, thumb pressure was applied to the syringe plunger to drive the dye into skin through the HNL MN. Thumb pressure was applied for 10 seconds to ensure injection and subsequent diffusion of the dye in the VE. The pressure was then removed from the syringe plunger, followed by the retraction of the HNL MN from the skin. Following the test, the skin was inspected under an optical microscope. An optical micrograph of the top view of the insertion/injection site on the skin is shown in Fig. 10. The opening in the SC was caused by successful insertion of the HNL MN into skin. The VE tissue underneath the SC was stained by the dye, as shown in Fig. 10, indicating that with the HNL MN being inserted into skin, the dye flowed into the VE through the lumen of the HNL MN, diffused in the VE, and then stained the VE with the application of thumb pressure. This preliminary manual injection test suggested the potential use of HNL MNs for drug delivery into skin.

IV. Conclusion

Conventional hypodermic needles have two key structural characteristics: a sharp beveled tip and a large side-terminated lumen. The sharp beveled tip reduces insertion force and pain perceived by patients, while the large side-terminated lumen provides a large fluid uptake area in the skin and reduces susceptibility to tissue clogging during insertion. Integration of these two key characteristics of HNs into MN design can potentially enhance MN performance. This work demonstrates the incorporation of these key structural features into polymer MNs in a batch-processing-compatible manner by exploiting a combination of UV lithography and micromolding.

This 6×6 HNL MN array consists of 1 mm tall high-aspect-ratio hollow SU-8 MNs with sharp beveled tips and 150 μm diameter side-opened lumens as well as a baseplate. A two-dimensional lithographic mask pattern and the topography of the micromold are utilized simultaneously to define the geometry of the beveled tip and the position of the lumen. The needle array was packaged and characterized for skin penetrability and fluidic functionality. A manual insertion test with excised porcine skin showed that the 6×6 HNL MN array was successfully inserted into skin with a successful insertion rate of 97% and no fracture or tip bending was observed under an optical microscope following the insertion. A microfluidic channel test indicated that at least 85% of the lumens were open.

Mechanical insertion characterization of HNL MNs was performed using excised porcine skin as a substrate and automatic force-displacement test stations. The insertion force of an HNL MN was determined to be 0.275 N, which is comparable to the insertion force of 0.284 N for a conventional 26G HN, indicating that HNL MNs exhibit comparable insertion performance to conventional 26G HNs. In comparison to the insertion force of 2.4 N for a PT MN in [18], HNL MNs exhibit superior insertion performance. With comparable tip diameters of PT MNs and HNL MNs, the approximately one-order-of-magnitude reduction in insertion force indicated that the tip geometry is an important factor in the insertion performance of MNs. With the fracture force of an HNL MN higher than 50 N and the insertion force of 0.275 N with excised porcine skin, the margin of safety for successful needle insertion prior to needle fracture is at least 180 for HNL MNs.

A preliminary manual injection test was performed using an HNL MN attached to a syringe to insert and then inject fluid into excised porcine skin. Following the test, staining of the VE tissues underneath the SC by the injected dye from the syringe was observed under an optical microscope in addition to an opening of the SC created by successful insertion of the HNL MN into skin. This demonstrated that the delivery of fluids into skin can be achieved through an HNL MN following the insertion into skin. Furthermore, the fluid resistance of an HNL MN was empirically estimated to be 5600 Pa/(ml/min), which is negligible in comparison to the required fluid pressure for saline injection into live human skin at a flow rate of 1.0 ml/min.

ACKNOWLEDGMENT

The authors would like to thank Dr. J.-W. Lee for the instruction on the Tricor force-displacement test station. Dr. Lee is in the Laboratory for Drug Delivery directed by Prof. M. Prausnitz at the Georgia Institute of Technology.

REFERENCES

[1] L. Vedrine, W. Prais, P. E. Laurent, C. Raynal-Olive, and M. Fantino, "Improving needle-point sharpness in prefillable syringes," *Med. Device Technol.*, vol. 14, no. 4, pp. 32–35, May 2003.

[2] A. Jaber, G. B. Bozzato, L. Vedrine, W. A. Prais, J. Berube, and P. E. Laurent, "A novel needle for subcutaneous injection of interferon beta-1a: Effect on pain in volunteers and satisfaction in patients with multiple sclerosis," *BMC Neurol.*, vol. 8, no. 1, p. 38, Oct. 2008.

[3] R. K. Sivamani, B. Stoeber, G. C. Wu, H. Zhai, D. Liepmann, and H. Maibach, "Clinical microneedle injection of methyl nicotinate: Stratum corneum penetration," *Skin Res. Technol.*, vol. 11, no. 2, pp. 152–156, May 2005.

[4] T. Frisk, N. Roxhed, and G. Stemme, "MEMS for medical technology applications," *Proc. SPIE*, vol. 6465, pp. 646513-1–646513-9, Feb. 2007.

[5] P. Zhang, C. Dalton, and G. A. Jullien, "Design and fabrication of MEMS-based microneedle arrays for medical applications," *Microsyst. Technol.*, vol. 15, no. 7, pp. 1073–1082, 2009.

[6] M. R. Prausnitz, J. A. Mikszta, M. Cormier, and A. K. Andrianov, "Microneedle-based vaccines," in *Vaccines for Pandemic Influenza*, R. W. Compans and W. A. Orenstein, Eds., 1st ed. Berlin, Germany: Springer-Verlag, 2009, pp. 369–393.

[7] M. R. Prausnitz, "Microneedles for transdermal drug delivery," *Adv. Drug Del. Rev.*, vol. 56, no. 5, pp. 581–587, Mar. 2004.

[8] Q. Zhu, V. G. Zarnitsyn, L. Ye, Z. Wen, Y. Gao, L. Pan, *et al.*, "Immunization by vaccine-coated microneedle arrays protects against lethal influenza virus challenge," *Proc. Nat. Acad. Sci. United States Amer.*, vol. 106, no. 19, pp. 7968–7973, May 2009.

[9] H. S. Gill, J. Soderholm, M. R. Prausnitz, and M. Sallberg, "Cutaneous vaccination using microneedles coated with hepatitis C DNA vaccine," *Gene Therapy*, vol. 17, no. 6, pp. 811–814, Jun. 2010.

[10] P. Van Damme, F. Oosterhuis-Kafeja, M. Van der Wielen, Y. Almagor, O. Sharon, and Y. Levin, "Safety and efficacy of a novel microneedle device for dose sparing intradermal influenza vaccination in healthy adults," *Vaccine*, vol. 27, no. 3, pp. 454–459, Jan. 2009.

[11] J. Gupta, E. Felner, and M. Prausnitz, "Minimally invasive insulin delivery in subjects with type 1 diabetes using hollow microneedles," *Diabetes Technol. Therapeutics*, vol. 11, no. 7, pp. 329–337, Jul. 2009.

[12] M. R. Prausnitz, S. Mitragotri, and R. Langer, "Current status and future potential of transdermal drug delivery," *Nature Rev. Drug Discovery*, vol. 3, no. 2, pp. 115–124, Feb. 2004.

[13] S. M. Bal, Z. Ding, E. van Riet, W. Jiskoot, and J. A. Bouwstra, "Advances in transcutaneous vaccine delivery: Do all ways lead to Rome?" *J. Controlled Release*, vol. 148, no. 3, pp. 266–282, Dec. 2010.

[14] H. J. G. E. Gardeniers, R. Luttge, E. J. W. Berenschot, M. J. de Boer, S. Y. Yeshurun, M. Hefetz, *et al.*, "Silicon micromachined hollow microneedles for transdermal liquid transport," *J. Microelectromech. Syst.*, vol. 12, no. 6, pp. 855–862, Dec. 2003.

[15] N. Baron, J. Passave, B. Guichardaz, and G. Cabodevila, "Investigations of development process of high hollow beveled microneedles using a combination of ICP RIE and dicing saw," *Microsyst. Technol.*, vol. 14, nos. 9–11, pp. 1475–1480, 2008.

[16] C. G. Li, C. Y. Lee, K. Lee, and H. Jung, "An optimized hollow microneedle for minimally invasive blood extraction," *Biomed. Microdevices*, vol. 15, no. 1, pp. 17–25, Feb. 2013.

[17] M. Matteucci, M. Fanetti, M. Casella, F. Gramatica, L. Gavioli, M. Tormen, *et al.*, "Poly vinyl alcohol re-usable masters for microneedle replication," *Microelectron. Eng.*, vol. 86, nos. 4–6, pp. 752–756, 2009.

[18] P.-C. Wang, S.-J. Paik, S. Chen, S. Rajaraman, S.-H. Kim, and M. G. Allen, "Fabrication and characterization of polymer hollow microneedle array using UV lithography into micromolds," *J. Microelectromech. Syst.*, vol. 22, no. 5, pp. 1041–1053, Oct. 2013.

[19] R. Luttge, E. J. W. Berenschot, M. J. de Boer, D. M. Altpeter, E. X. Vrouwe, A. van den Berg, *et al.*, "Integrated lithographic molding for microneedle-based devices," *J. Microelectromech. Syst.*, vol. 16, no. 4, pp. 872–884, Aug. 2007.

[20] P.-C. Wang, S.-J. Paik, J. Kim, S.-H. Kim, and M. G. Allen, "Hypodermic-needle-like hollow polymer microneedle array using UV lithography into micromolds," in *Proc. IEEE 24th Int. Conf. Micro Electro Mech. Syst.*, Cancun, Mexico, Jan. 2011, pp. 1039–1042.

[21] B. P. Chaudhri, F. Ceyssens, H. P. Neves, A. La Manna, C. Van Hoof, and R. Puers, "Out-of-plane high strength polymer microneedles for transdermal drug delivery," in *Proc. 33rd Annu. Int. Conf. IEEE Eng. Med. Biol. Soc.*, Boston, MA, USA, Sep. 2011, pp. 3680–3683.

[22] F. Ceyssens, B. P. Chaudhri, C. Van Hoof, and R. Puers, "Fabrication process for tall, sharp, hollow, high aspect ratio polymer microneedles on a platform," *J. Micromech. Microeng.*, vol. 23, no. 7, p. 075023, Jun. 2013.

[23] Y.-K. Yoon, J.-H. Park, and M. G. Allen, "Multidirectional UV lithography for complex 3-D MEMS structures," *J. Microelectromech. Syst.*, vol. 15, no. 5, pp. 1121–1130, Oct. 2006.

[24] S. Rajaraman, J. A. Bragg, J. D. Ross, and M. G. Allen, "Micromachined three-dimensional electrode arrays for transcutaneous nerve tracking," *J. Micromech. Microeng.*, vol. 21, no. 8, p. 085014, Jun. 2011.

[25] T. C. Merkel, V. I. Bondar, K. Nagai, B. D. Freeman, and I. Pinnau, "Gas sorption, diffusion, and permeation in PDMS," *J. Polymer Sci., B, Polymer Phys.*, vol. 38, no. 3, pp. 415–434, Feb. 2000.

[26] A. Arora, M. R. Prausnitz, and S. Mitragotri, "Micro-scale devices for transdermal drug delivery," *Int. J. Pharmaceutics*, vol. 364, no. 2, pp. 227–236, Dec. 2008.

[27] P.-C. Wang, B. A. Wester, S. Rajaraman, S.-J. Paik, S.-H. Kim, and M. G. Allen, "Hollow polymer microneedle array fabricated by photolithography process combined with micromolding technique," in *Proc. 31st Annu. Int. Conf. IEEE Eng. Med. Biol. Soc.*, Minneapolis, MN, USA, Sep. 2009, pp. 7026–7029.

[28] J. M. Gere and B. J. Goodno, *Mechanics of Materials*, 8th ed. Stamford, CT, USA: Cengage Learning, 2012, pp. 68–69.

[29] D. S. Viswanath, T. K. Ghosh, D. H. L. Prasad, N. K. Dutt, and K. Y. Rani, *Viscosity of Liquids: Theory, Estimation, Experiment, and Data*. Berlin, Germany: Springer-Verlag, 2007, pp. 11–14.

[30] J. Gupta, "Microneedles for transdermal drug delivery in human subjects," Ph.D. dissertation, School Chem., Biomolecular Eng., Georgia Inst. Technol., Atlanta, GA, USA, 2009.

Po-Chun Wang received the B.S. degree in electronics engineering from National Chiao-Tung University, Hsin-Chu, Taiwan, in 1997 and the M.S. degree in electrical engineering from Pennsylvania State University, State College, PA, in 2002. From 2002 to 2007, he was with Taiwan Semiconductor Manufacturing Company, Hsin-Chu, Taiwan, where he enhanced yield and performance of silicon CMOS integrated circuits. He is currently working toward the Ph.D. degree in electrical and computer engineering at the Georgia Institute of Technology, Atlanta, GA. His Ph.D. research focuses on fabrication and characterization of micromachined hollow polymer needle arrays for drug delivery into skin.

Seung-Joon Paik received the B.S. degree from the School of Electrical Engineering, and the M.S. and Ph.D. degrees in electrical engineering and computer science from Seoul National University, Seoul, Korea, in 1999, 2001, and 2005, respectively. He was with the Automation and Systems Research Institute, Seoul National University, as a Postdoctoral Fellow from 2005 to 2007, and with SML Electronics, Inc., Seoul, from 2007 to 2008. In 2008, Dr. Paik joined the Micro Sensors and Micro Actuators Laboratory (MSMA), Georgia Institute of Technology as a Postdoctoral Fellow and led the biomedical microdevices research group. Since 2013, he is a member of the Research Faculty at the Institute for Electronics and Nanotechnology (IEN), Georgia Institute of Technology, and has researched biosensors based on microfabrication technology and coordinated the operations of an instructional laboratory for CMOS and MEMS courses. Dr. Paik has published more than 60 reviewed journal and conference articles, and has invented 13 patents. His research interests include microsystem design and fabrication, process integration, and nano-scale structures in the applications of sensors and actuators, biomedical devices, and energy storage/conversion devices.

Seong-Hyok Kim received his B.S.E. and M.S. degrees from the Department of Electrical Engineering, Seoul National University in 1996 and 1998, respectively. He received the Ph. D. degree in electrical engineering and computer science from Seoul National University in 2002. After joining LG Electronics Institute of Technology as a Senior Research Engineer in 2002, he participated in the design and fabrication of a wide variety of MEMS devices for portable electronics. In 2005, Dr. Kim joined the Micro Sensors and Micro Actuators Laboratory (MSMA), Georgia Institute of Technology as a Postdoctoral Fellow and led the PowerMEMS research group at the MSMA lab. Since he became a Research Engineer II in 2007, Dr. Kim led the MSMA laboratory's research projects encompassing micro sensors and actuators, nanomaterials, power passives, bio-medical microdevices, etc. Since 2010, he has been the Principal Research Engineer at LG Electronics Mobile Communication Company. Dr. Kim has published more than 50 peer-reviewed journal and conference articles, and holds 29 Korean/International patents in the field of MEMS, including power MEMS, bio MEMS, polymer MEMS, optical MEMS, and MEMS sensors and actuators.

Mark G. Allen (M'89-SM'04-F'11) received the B.A. degree in chemistry, the B.S.E. degree in chemical engineering, and the B.S.E. degree in electrical engineering from the University of Pennsylvania, and the S.M. and Ph.D. (1989) degrees from the Massachusetts Institute of Technology. In 1989 he joined the Faculty of the School of Electrical and Computer Engineering, Georgia Institute of Technology, where he currently holds the rank of Regents' Professor and the J.M. Pettit Professorship in Microelectronics, as well as a joint appointment in the School of Chemical and Biomolecular Engineering. His research interests include the development and application of new micro- and nanofabrication technologies, as well as MEMS. He is Editor-in-Chief of the *Journal of Micromechanics and Microengineering*, previous Co-Chair of the IEEE/ASME MEMS Conference, and a Fellow of the IEEE.